Supporting Information

Design and Synthesis of Two-Dimensional Covalent Organic Frameworks with Four-Arm Cores: Prediction of Remarkable Ambipolar Charge-Transport Properties

Simil Thomas,[†a] Hong Li,[†a] Raghunath R. Dasari,[†a] Austin M. Evans,[b] Ioannina Castano,[b] Taylor G. Allen,[c] Obadiah G. Reid,[c,d] Garry Rumbles,[c,d] William R. Dichtel,[b] Nathan C. Gianneschi,[b,e,f] Seth R. Marder[*a] , Veaceslav Coropceanu,[*a] and Jean-Luc Brédas[*a]

[a]School of Chemistry and Biochemistry, Center for Organic Photonics and Electronics (COPE), Georgia Institute of Technology, Atlanta, GA, 30332-0400, United States.

[b]Department of Chemistry, Northwestern University, Evanston, Illinois, 60208, United States.

[c]National Renewable Energy Laboratory, 15013 Denver West Parkway, Golden, Colorado 80401, United States.

[d]Renewable and Sustainable Energy Institute, Department of Chemistry, University of Colorado, Boulder, CO 80309, United States.

[e]Department of Materials Science and Engineering, Northwestern University, Evanston, IL 60208, United States.

[f]Department of Biomedical Engineering, Northwestern University, Evanston, IL 60208, United States.

I. Materials and Instrumentation

All reagents were purchased from commercial sources and used without further purification. [5, 10, 15, 20-*Tetrakis*(ethynyl)porphyrinato]zinc(II) monomer, ZnTEP,[1,2] and its precursors [5, 10, 15, 20-*tetrakis*-(triisopropylsilylethynyl)porphyrinato]zinc(II),[3] 5, 10, 15, 20-*tetrakis*-triisopropylsilylethynylporphyrin,[3] and 3-triisoporpylsilylprop-2-ynal[4-5] were synthesized using literature procedures. Poly(methylmethacrylate) (PMMA, Mw ~15 kDa by GPC Sigma Aldrich 200336), polystyrene (~280 kDa by GPC Sigma Adlrich 182427), and [5, 10, 15, 20-tetraphenylporphyrinato]zinc(II) (ZnTPP, Sigma Aldrich 252166) were used as received. Column chromatography was carried out using silica gel (46-63 µm, Sorbent) as the stationary phase, and thin-layer chromatography (TLC) was performed on precoated silica-gel plates (0.25 mm thick, 60F254, EMD, Germany) and visualized under UV light. The ^{1}H and $^{13}C\{^{1}H\}$ NMR spectra were measured on Varian Mercury 300 MHz and 400 MHz spectrometers. The chemical shift values were referenced with the solvent residual proton signal or the solvent carbon signal as internal standard. Infrared spectra were measured on Shimadzu IRPrestige-21 Fourier Transform Infrared Spectrophotometer. Mass spectra were measured on an Applied Biosystems 4700 Proteomics Analyzer using MALDI or a Micromass AutoSpec M using electron impact (EI) mode. Elemental analyses were carried out by Atlantic Microlabs using a LECO 932 CHNS elemental analyzer. Inductively coupled plasma mass spectrometry (ICP-MS) analyses were performed on NexION 300Q, PerkinElmer instrument.

Powder X-ray Diffraction: X-ray diffraction patterns were recorded on a Panalytical Empyrean Powder X-Ray Diffractometer in 2θ medium resolution Brag Brentano geometry employing Cu Kα line focused radiation at 40 kV, 40 mA power and equipped with a PIXcel Medipix3 3D detector. No sample grinding was used prior to analysis unless otherwise noted. Samples were observed using a continuous 2θ scan from 1.0 – 40º for approximately 60 minutes.

Crystallite Modeling. Crystal modeling of the COF structures was carried out using the Materials Studio (ver.5.0) suite of programs by Accelrys. The initial structures were constructed piecewise starting with a primitive tetragonal unit cell with a P4 space group. The cell parameter was estimated according to the distance between the center of the vertices for each COF, and c parameter was chosen as 3.35 Å, which has been observed for similar materials. The structures were optimized using a Geometry Optimization routine including energy minimization with cell parameters optimization, using the parameters from the Universal Force Field. Calculation of the simulated powder diffraction patterns and Pawley refinements were performed in the Materials Studio Reflex Plus Module using a Bragg-Brentano geometry. The observed diffraction patterns were subjected to a polynomial background subtraction and then to Pawley refinement wherein peak profile were refined using the Pseudo-Voigt peak shape function and asymmetry was corrected using the Berar-Baldinozzi function. Crystallite size was then estimated by the LeBail method which was Pawley refined to the experimental data. Surface area calculations were carried out using a Connolly surface calculation using the appropriate parameters for nitrogen as the adsorbed gas.

Gas Adsorption. Gas adsorption isotherms were conducted on a Micromeritics ASAP 2420 Accelerated Surface Area and Porosity Analyzer. Typically, 20-50 mg samples were transferred to dried and tared analysis tubes equipped with filler rods and capped with a Transeal. The samples were heated to 120 °C at a rate of 5 °C/min and evacuated until the outgas rate was ≤0.3 μmHg/min (holding the samples at 120 °C overnight was sufficient), at which point the tube was weighed again to determine the mass of the activated sample. The tube was then transferred to the analysis port of the instrument. UHP-grade (99.999% purity) N_2 was used for all adsorption measurements. N_2 isotherms were generated by incremental exposure to nitrogen up to 760 mm of Hg (1 atm) in a liquid nitrogen (77 K) bath. Oil-free vacuum pumps and oil-free pressure regulators were used for all measurements. Brunauer-Emmett-Teller (BET) surface areas were calculated from the linear region of the N_2 isotherm at 77 K within the pressure range P/P0 of 0.05 – 0.10 so that the linear model fit had an R^2 of greater than .999.

Transmission Electron Microscopy (TEM) Sample Preparation. Sample solutions (~1 mg/mL) were prepared by suspending the ZnPor-COF powder in 50 vol% ethanol 50 vol% water and sonicating the solution for ~30 minutes. TEM grids were prepared by drop-casting ~4 μL (using a micropipette) of the sample solution onto lacey-carbon substrate (Cu, 400 mesh) TEM grids (Ted Pella, Redding, CA). The droplets were allowed to sit on the grids in ambient conditions for ~10s, and were then wicked dry with filter paper.

TEM Characterization. TEM images were taken using a JEOL (JEOL USA, Inc., Peabody, MA) ARM300F GrandARM TEM operating at 300 keV with a Gatan (Gatan, Inc., Pleasanton, CA) OneView-IS camera (FEG Emission: 15 μA, spot size 4, 100 μm CL aperture, exposure time 0.5 s). Selected-area electron diffraction (SAED) images were taken with diffraction imaging mode (10 μm selected area aperture, camera length of 150 cm, exposure time 2 s). All image acquisition was done using Digital Micrograph which is part of the Gatan Microscopy Suite (GMS 3).

Substrate Cleaning. Quartz substrates for microwave conductivity measurements were cleaned by first sonicating in acetone for 5 minutes and then treating with ozone plasma for 5 minutes. Substrates were used for film making immediately to avoid surface contamination.

ZnPor-COF, ZnTPP, ZnTEP Film Processing. ZnPor-COF-PMMA films were made by adding 5 mg of ZnPor-COF to 1 mL of a 100 mg/mL solution of PMMA in chloroform and stirred vigorously for 30 min, protected from ambient light. To avoid settling, 100 L aliquots of the COF-PMMA solution were quickly drop casted onto a clean quartz slide such that the entire surface was flooded. ZnPor-COF-polystyrene films were made similarly, where 5 mg of ZnPor-COF powder was added to 1 mL of 20 mg/mL solution of polystyrene in chloroform. ZnTPP, and ZnTEP neat films were made by spin coating 5 mg/mL solutions in HPLC grade chloroform and THF, respectively, at 1000 RPM for 30 s (Ramp = 1000 RPM/s).

Absorption Spectroscopy. Transmission spectra of neat ZnTPP, ZnTEP and ZnPor-COF-polymer films were acquired using a Cary 6000i absorption spectrometer. Scans were acquired from 600-

1800 nm with 1 nm resolution, using a clean quartz slide as the reference. Given the scattering nature of the ZnPor-COF-polymer films, absorption spectra were also taken with an integrating sphere to exclude scattering contributions to the spectrum. This system consisted of an Ocean Optics halogen lamp (DH-2000) fiber-coupled to an integrating sphere (LabSphere model) whose output is relayed via optical fiber to the liquid nitrogen cooled Si and InGaAs CCDs of a Princeton photoluminescence spectrometer (SpectraPro HRS-300). Spectra were acquired with a 150 line/mm grating with 800 nm blaze, 250 micron slit width, 300 ms exposure (1 s for NIR), average of 20 frames. For visible-NIR scans, a 550 nm long pass filter was used to avoid secondary diffraction signal at ca. 1000 nm. Similarly, a 950 nm long pass filter was used in the NIR spectra. In agreement with the transmission data, the integrating sphere absorption spectra show a long absorption tail into the NIR. Discontinuities in the NIR spectra are thought to be the result of fiber losses that are not subtracted completely by normal reference methods.

Flash-Photolysis Time-Resolved Microwave Conductivity (fp-TRMC). Our fp-TRMC measurement system and methods has been described in detail elsewhere.[6,7] Photoexcitation was accomplished using a Nd:YAG (Spectraphysics Quanta Ray SP Pro 230-30H) laser with 9 W of 355 nm at 30 Hz to pump an OPO (Spectraphysics GWU PremiScan ULD/500) with output over the range of 410-2500 nm with 7 ns pulses (ca. 3 W output, varies by wavelength). Samples were purged continuously with nitrogen during measurements. Blank quartz substrates were used to determine the lower limit of measurable yield-mobility products. ZnPor-COF-polymer films were excited at 700 nm with fluences in the range of ca. 0.2 – 4 x 10^{15} photons/cm^2. ZnTPP neat films were excited at 430, 550, and 700 nm with similar fluences. Each transient was acquired for 30,000 shots or until S/N = 10. Data was processed by a custom global fitting routine in Igor Pro 8 using a biexponential fit. Yield mobility products at each fluence were extracted by summation the amplitudes of the optimized fit coefficients. The actual monomer, ZnTEP, was not measured because of its solubility and film formation issues (i.e. thinness and scattering). ZnTPP made better films due to better solubility and wetting in chloroform solution. Since the structures and absorption spectra for ZnTPP and ZnTEP were similar (see Figure S17), ZnTPP was expected to give a reasonable estimate of how the photoconductivity differed between ZnPor-COF and a "monomer-like" compound.

Photoexcited Steady-State Microwave Conductivity (PSSMC): Details for the SSMC system will be presented in an upcoming publication: O. G. Reid, H. Zhang, D. Vigil-Fowler, S. J. Yoon, Y. H. Lee, E. M. Miller, and J. L. Blackburn. "Direct Creation of Free Charge Carriers in Monolayer WS2 via Optically Active Defect States". *In Preparation.* Data was analyzed in Igor Pro 8. Representative plots of differential voltage and light source photon flux as a function of wavelength are provided. ZnPor-COF-polymer films showed broadband photoconductivity, which resulted in the differential voltage signal tracking with the photon flux of the lamp output (see Figures S18 and S19). Blank quartz, neat PMMA, neat polystyrene, and neat ZnTPP films were measured to gauge the polymer and monomer-like background signals, respectively. No signal was obtained for blank quartz, PMMA, polystyrene, or ZnTPP – see Figure S19b for representative quartz spectrum. Although baseline offsets differed slightly between the non-ZnPor-COF

samples, the noise level was repeatable (ca. $\pm$ 20 nV). Like Figure S19b, this resulted in flat scans which fluctuated around their respective baseline offsets.

Synthesis

1. [5, 10, 15, 20-*Tetrakis*(ethynyl)porphyrinato]zinc(II): Synthesis of zincporphyrin monomer **1** was carried out as per a reported procedure.[1] ^{1}H and ^{13}C NMR characterization is consistent with that reported in the literature.[1] HRMS (MALDI) calcd for $C_{28}H_{12}N_4Zn$ (M^+), 406.1218; found 406.1223. Anal. Calcd. for $C_{28}H_{12}N_4Zn._{2/3}H_2O$: C, 69.80; H, 2.79; N, 11.63. Found: C, 69.60; H, 2.81; N, 11.23.

2. Zincporphyrin COF, **2**. A 100 mL 2-neck flask was charged with [5, 10, 15, 20-tetrakis(ethynyl)porphyrinato]zinc(II) (0.05 g, 0.10 mmol), 1,4-dioxane (25 mL) and the resulting suspension was sonicated at room temperature for 90 minutes to dissolve zincporphyrin in 1,4-dioxane. *N*,*N'*-Diisopropylamine (8 mL), and copper(II)acetate (0.06 g, 0.30 mmol) in 8 mL 1,4-dioxane, were added. The reaction mixture was heated at 90 ^{o}C for 72 h without stirring. The flask was removed from the heating source, the resulting suspension was allowed to cool, and was filtered the reaction mixture through a Büchner funnel. The dark color precipitate was washed with 1,4-dioxane (50 mL). The solid was collected, and stirred in an Erlenmeyer flask in hot 1,4-dioxane (70 mL at 90 °C for 15 min), and filtered while hot. The collected precipitate was washed with hot methanol (70 mL at 70 ^{o}C) in a similar manner. Finally, the dark precipitate was collected by filtration, and dried at 100 °C for 24 h under vacuum (~30 mTorr). Yield: 0.045 g (90%). ICP-MS (wt%): Zn, 5.19% (13.92%, theoretical); Cu, 4.89%.

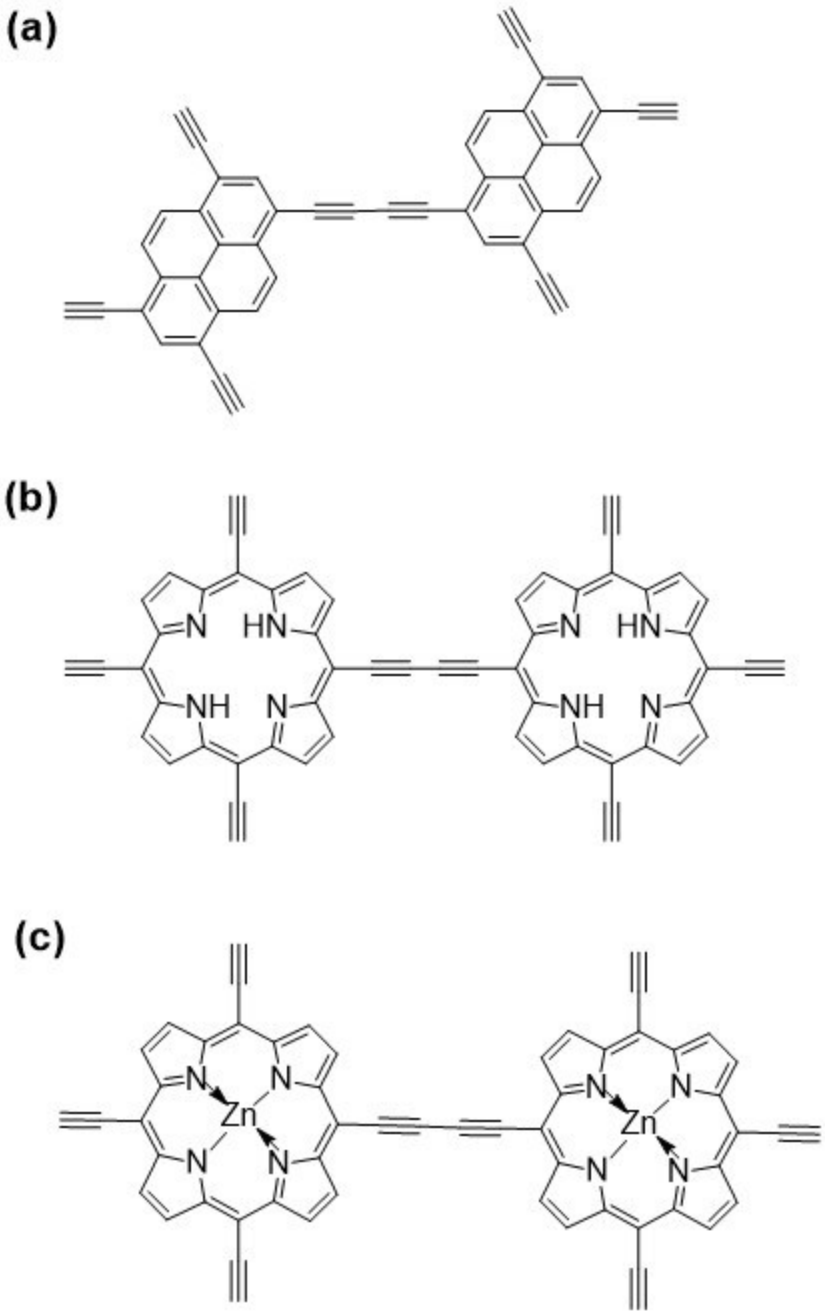

Figure S1. Chemical structures of the diacetylene-linked pyrene (a), porphyrin (b), and zinc-porphyrin (c) dimer models considered in the mixed-valence calculations.

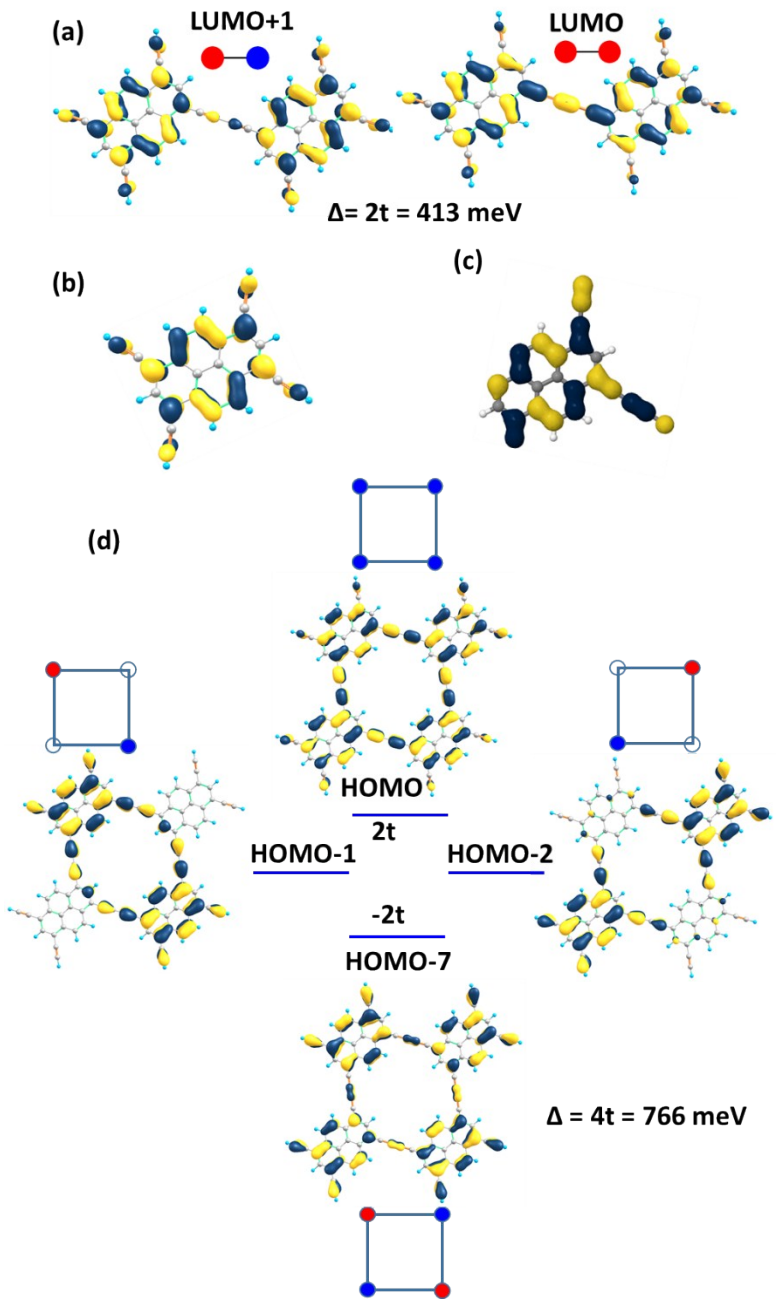

Figure S2. (a) Illustration of the LUMO and LUMO+1 wavefunctions in the Pyr-COF dimer and estimation of the transfer integrals (t) for electrons, based on the energy-splitting approach; Δ denotes the difference between the LUMO and LUMO+1 energies of the dimer; the red and blue dots express the symmetry of the tight-binding wavefunctions. (b) LUMO of the pyrene building block. (c) Wavefunction of the conduction band minimum of the 2D Pyr-COF at the Γ-point. (d) Illustration of the HOMO, HOMO-1, HOMO-2 and HOMO-7 wavefunctions in the Pyr-COF tetramer and estimation of the transfer integrals (t) for holes, based on the energy-splitting approach; Δ denotes the difference between the HOMO and HOMO-7 energies of the tetramer; the red and blue dots express the symmetry of the tight-binding wavefunctions.

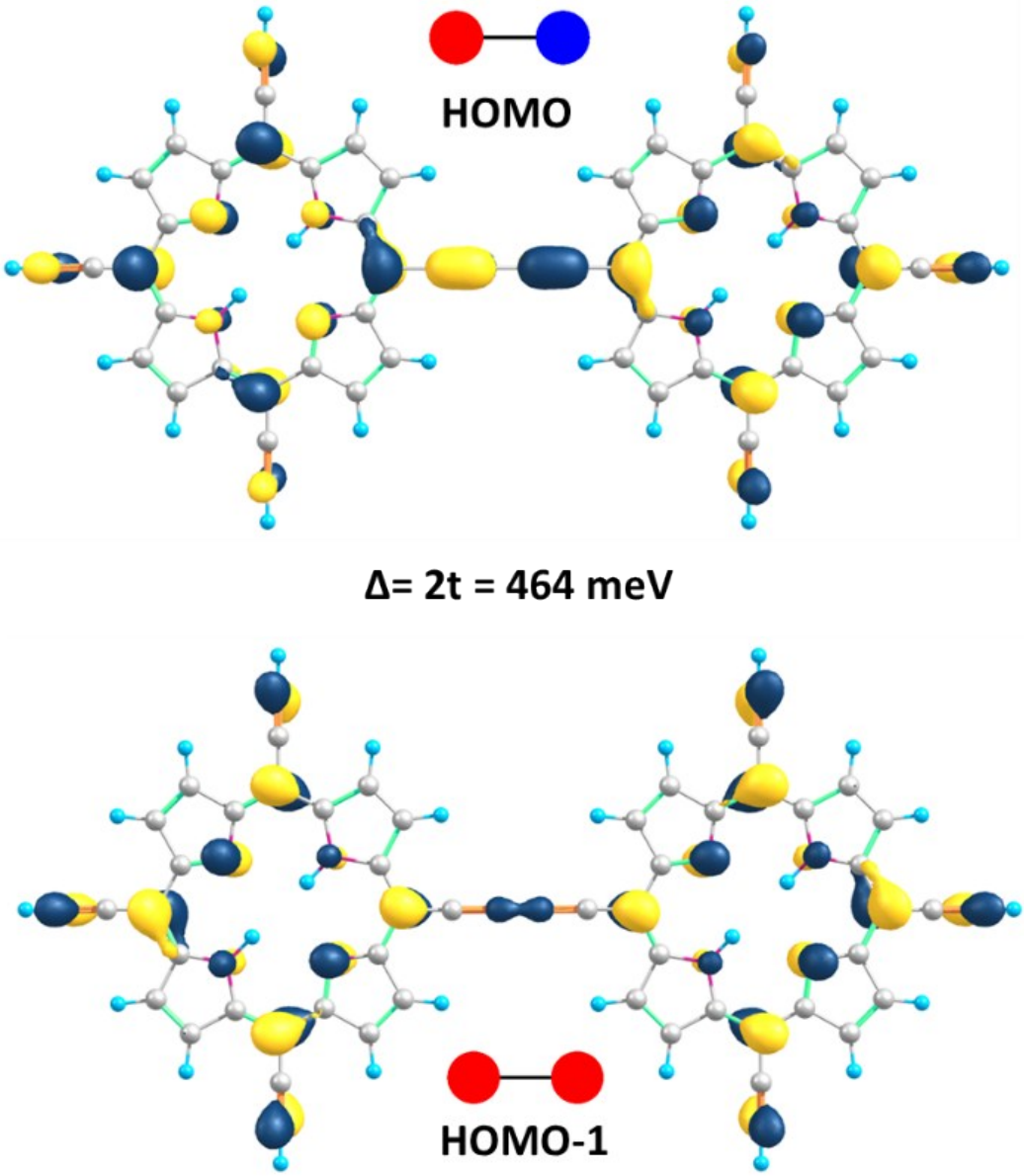

Figure S3. Illustration of the HOMO and HOMO-1 wavefunctions in the Por-COF dimer and estimation of the transfer integrals (t) for holes, based on the energy-splitting approach; Δ denotes the difference between the HOMO and HOMO-1 energies of the dimer; the red and blue dots express the symmetry of the tight-binding wavefunctions.

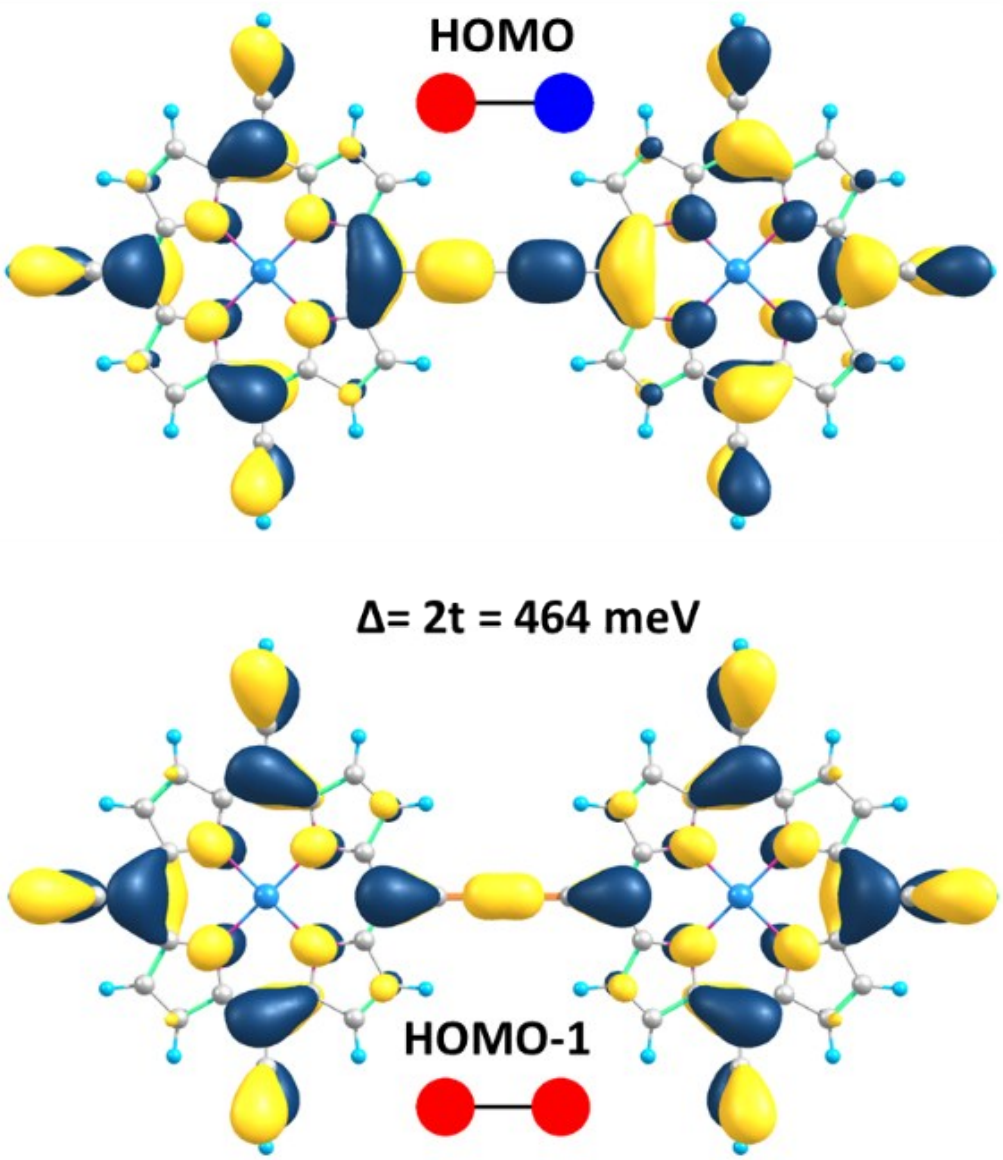

Figure S4. Illustration of the HOMO and HOMO-1 wavefunctions in the ZnPor-COF dimer and estimation of the transfer integrals (t) for holes, based on the energy-splitting approach; Δ denotes the difference between the HOMO and HOMO-1 energies of the dimer; the red and blue dots express the symmetry of the tight-binding wavefunctions.

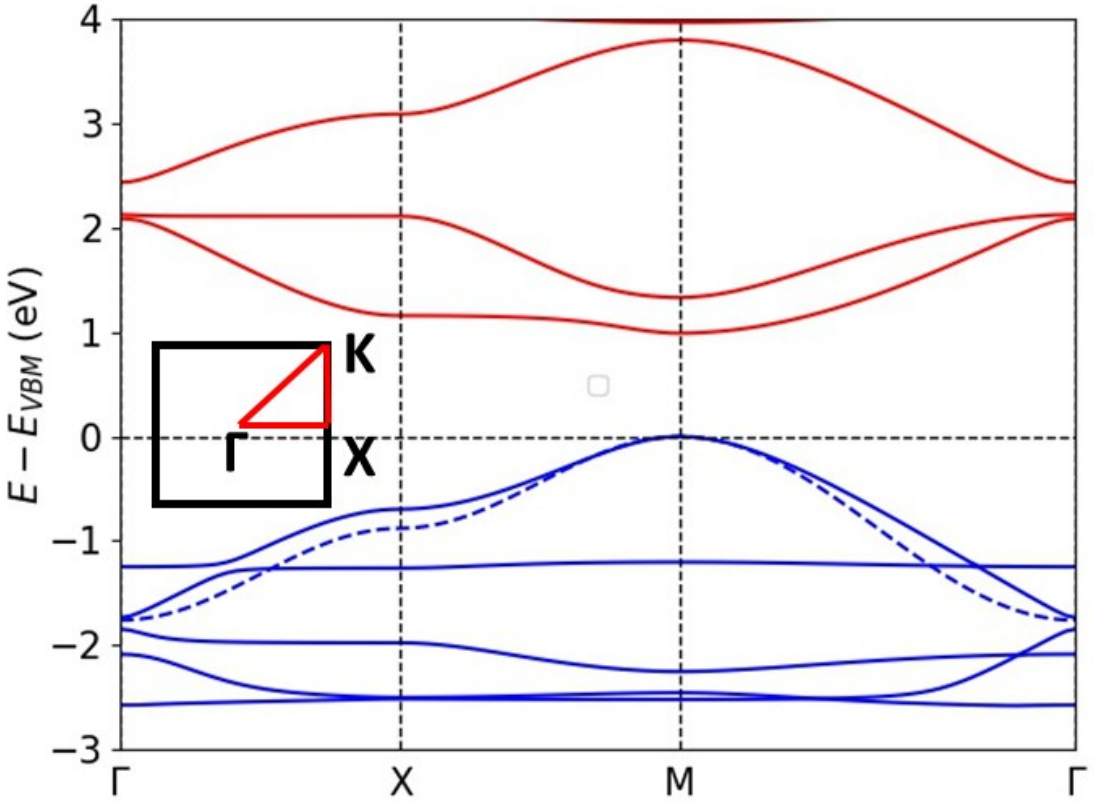

Figure S5. DFT-PBE0-calculated electronic band structures of Por-COF where the dotted lines correspond to the tight-binding band structure (the Brillouin zones and high-symmetry points are shown in the insets). The valence and conduction bands are colored in blue and red, respectively.

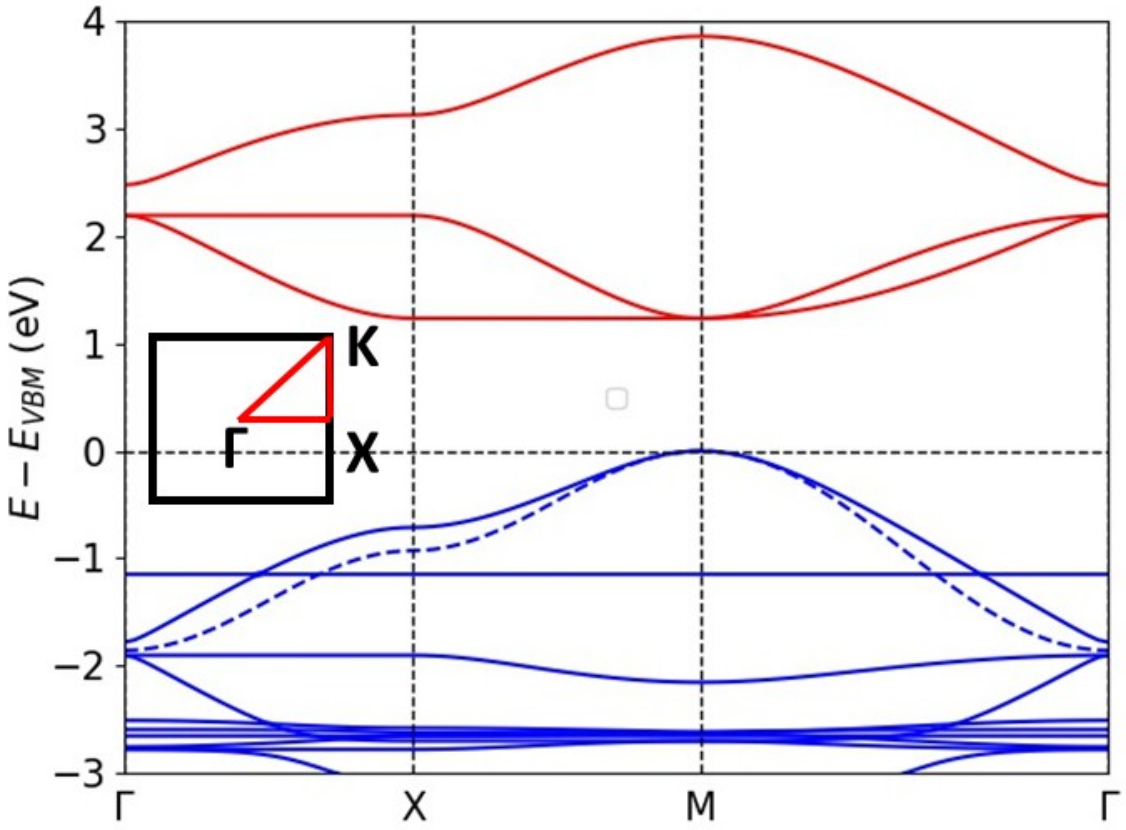

Figure S6. DFT-PBE0-calculated electronic band structures of ZnPor-COF where the dotted lines correspond to the tight-binding band structure (the Brillouin zones and high-symmetry points are shown in the insets). The valence and conduction bands are colored in blue and red, respectively.

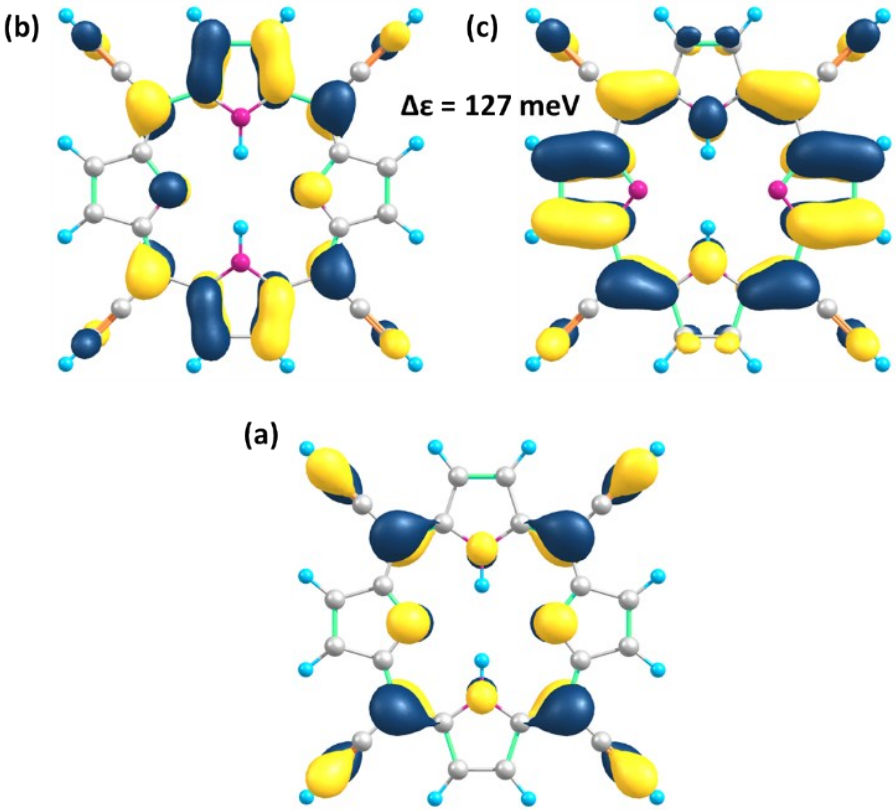

Figure S7. Illustration of: (a) the HOMO; (b) the LUMO; and (c) the LUMO+1 of the porphyrin core. Δε is the energy difference between LUMO and LUMO+1.

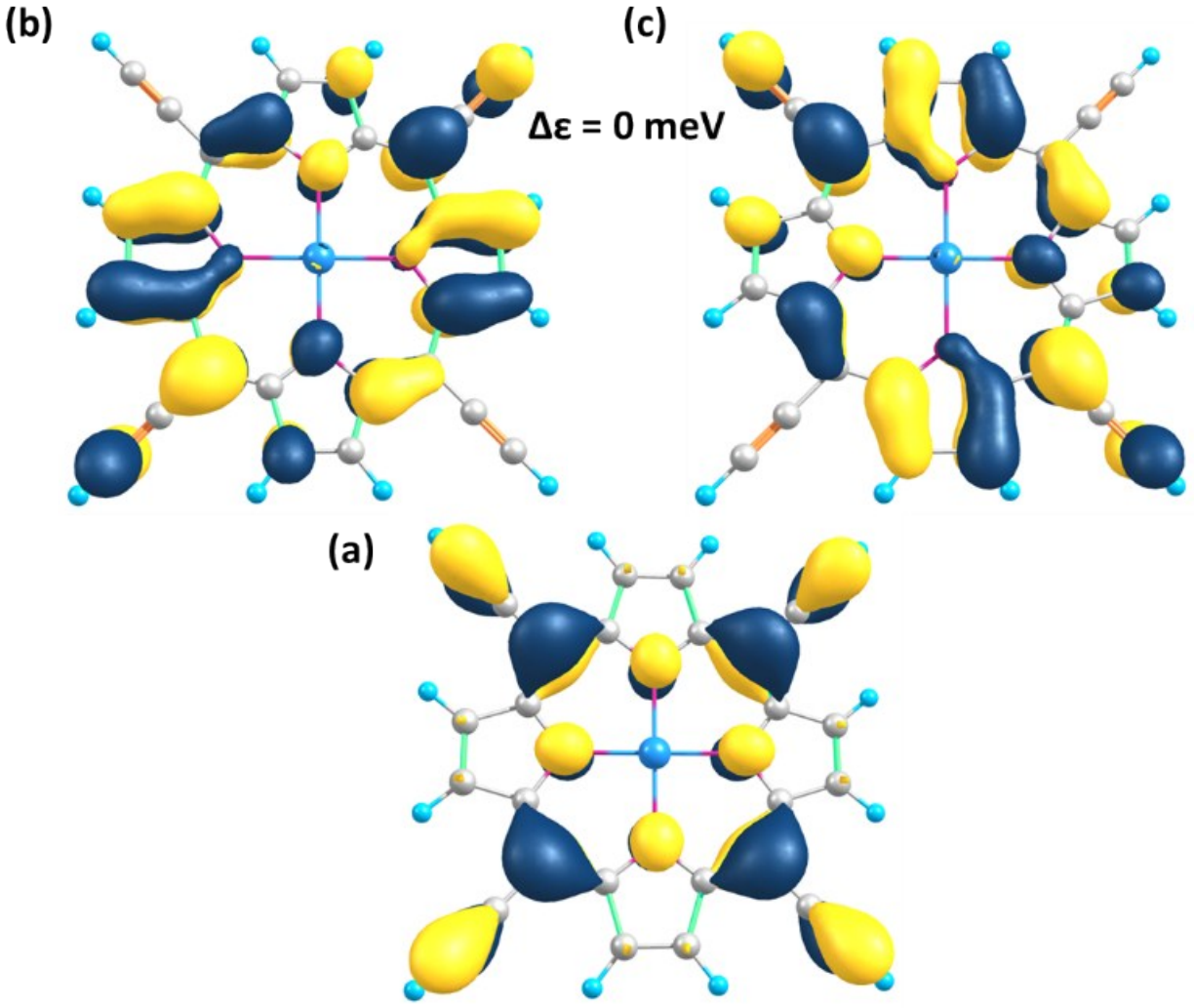

Figure S8. Illustration of: (a) the HOMO; (b) the LUMO; and (c) the LUMO+1 of the porphyrin core. Δε is the energy difference between LUMO and LUMO+1.

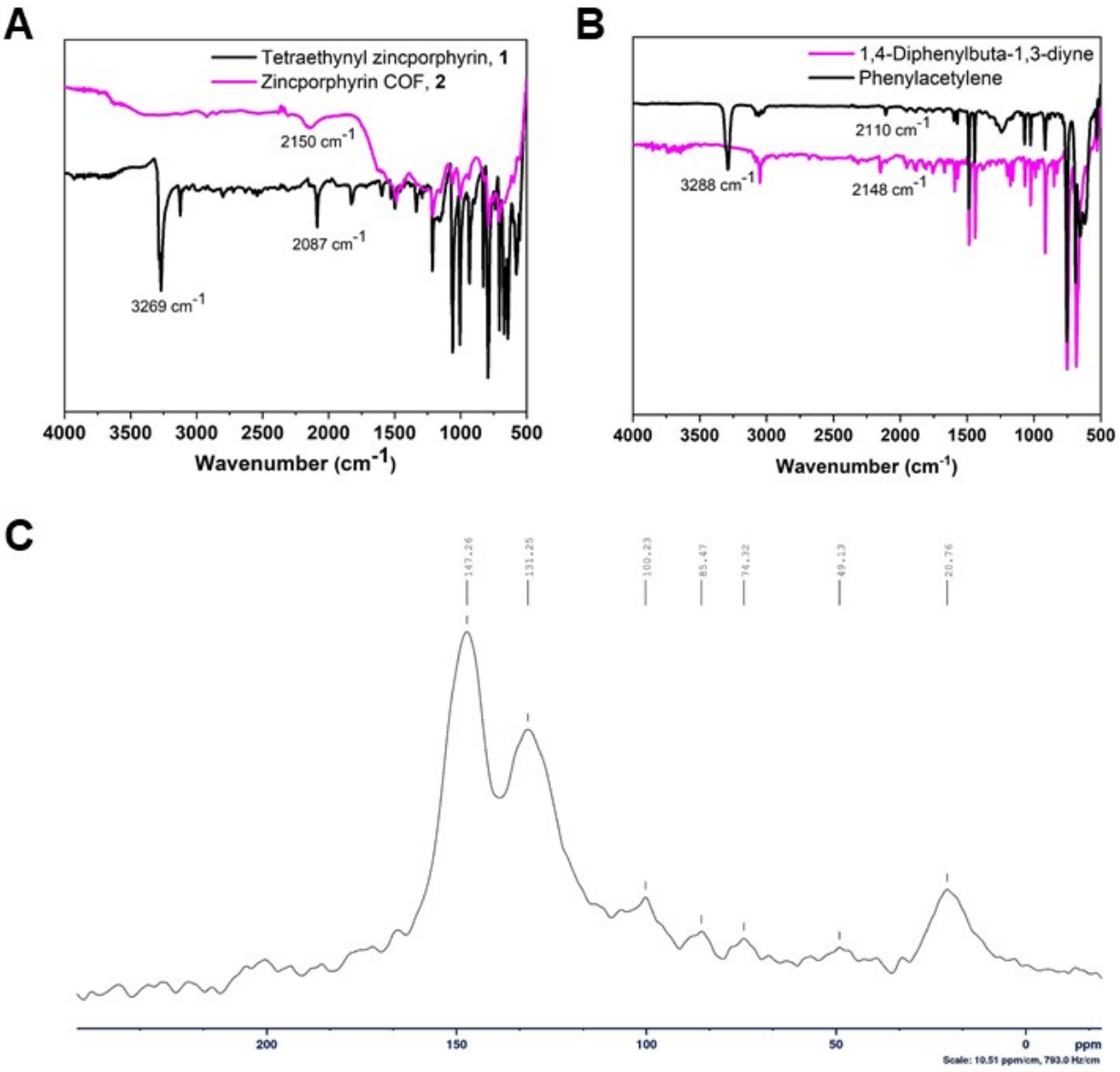

Figure S9. Infrared spectra of (A) **2** and tetraethynylzincporphyrin monomer; and (B) 1,4-diphenylbuta-1,3-diyne and phenylacetylene monomer. (C) CP/MAS ^{13}C NMR spectra of **2**.

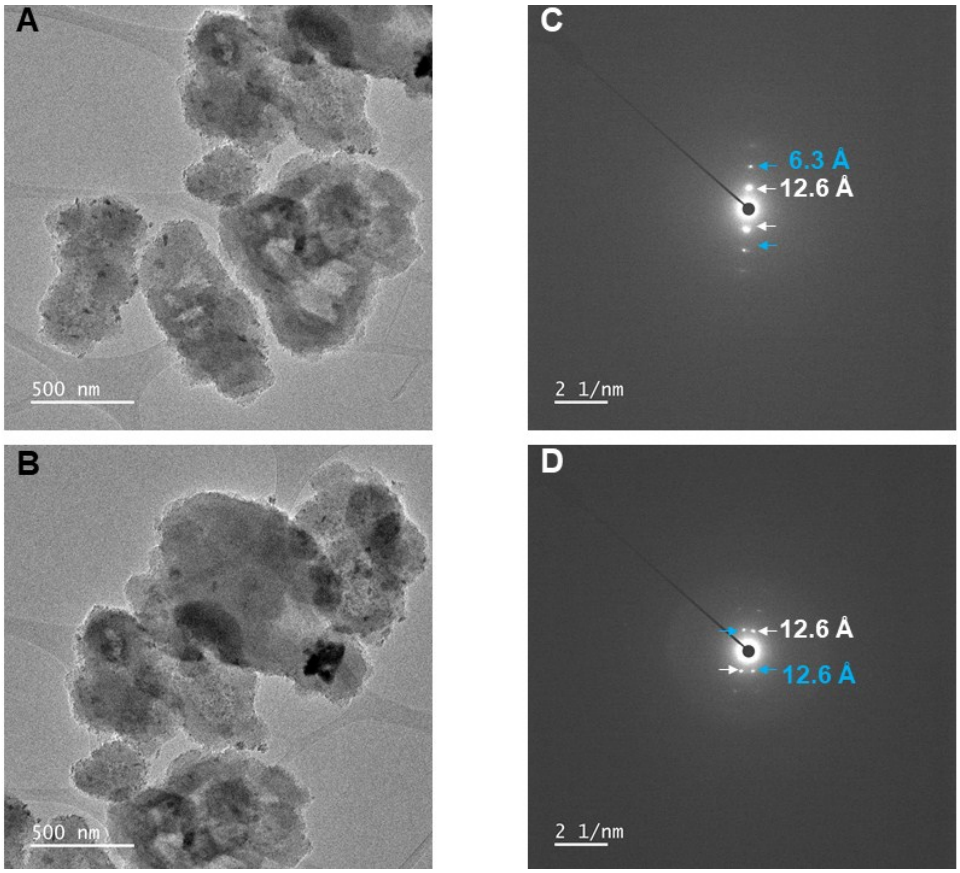

Figure S10. (A-B) Low-resolution images of ZnPor-COF particles and (C-D) their associated SAED patterns.

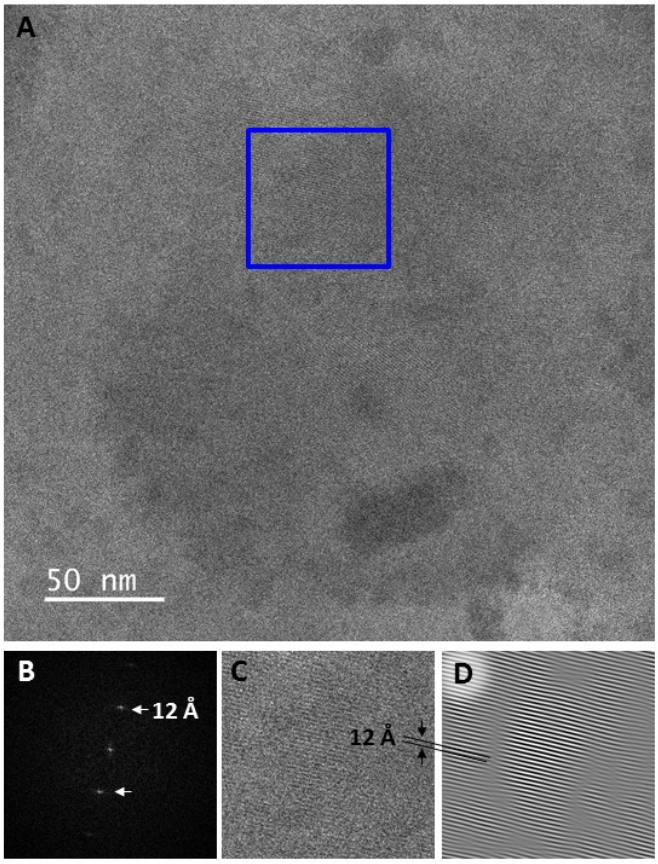

Figure S11. (A) High-resolution image of a ZnPor-COF particle. (B) FFT of the boxed region of A which demonstrates a consistent lattice spacing that is in good agreement with bulk diffraction data. (C) Cropped image of the boxed region in A showing lattice features. (D) Bandpass filtered image of C showing the lattice more clearly.

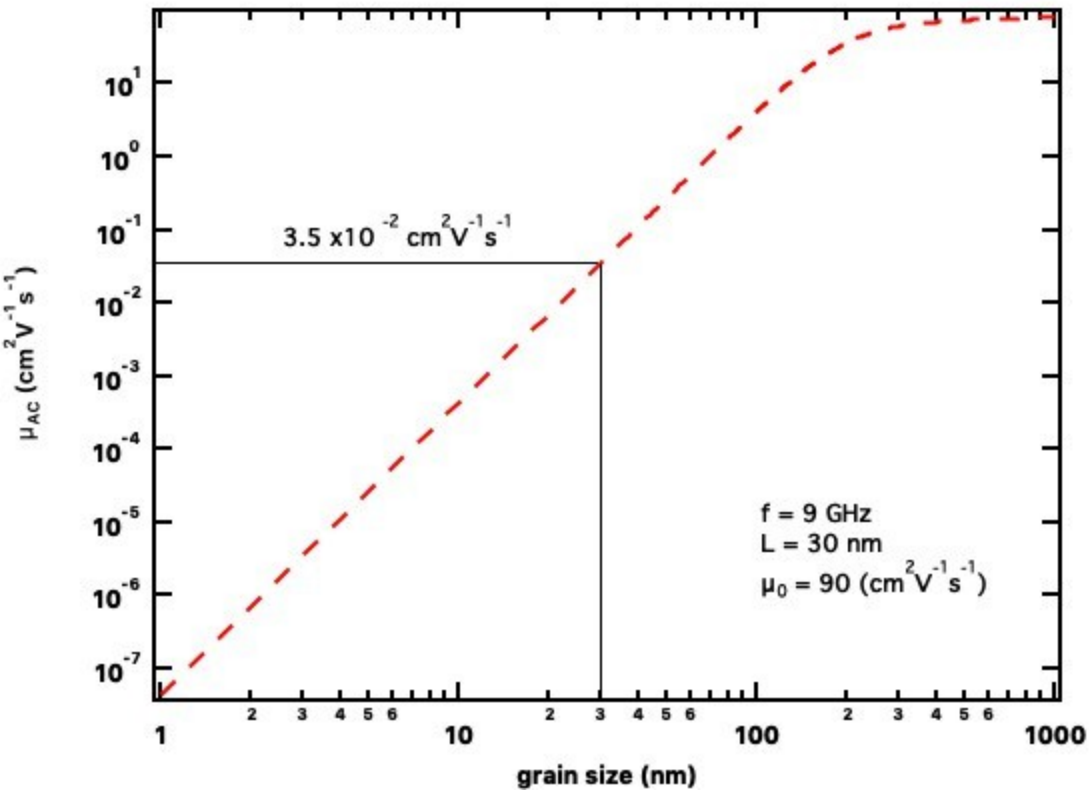

Figure S12. A Kubo plot of calculated AC mobility vs grain size of ZnPor-COF.

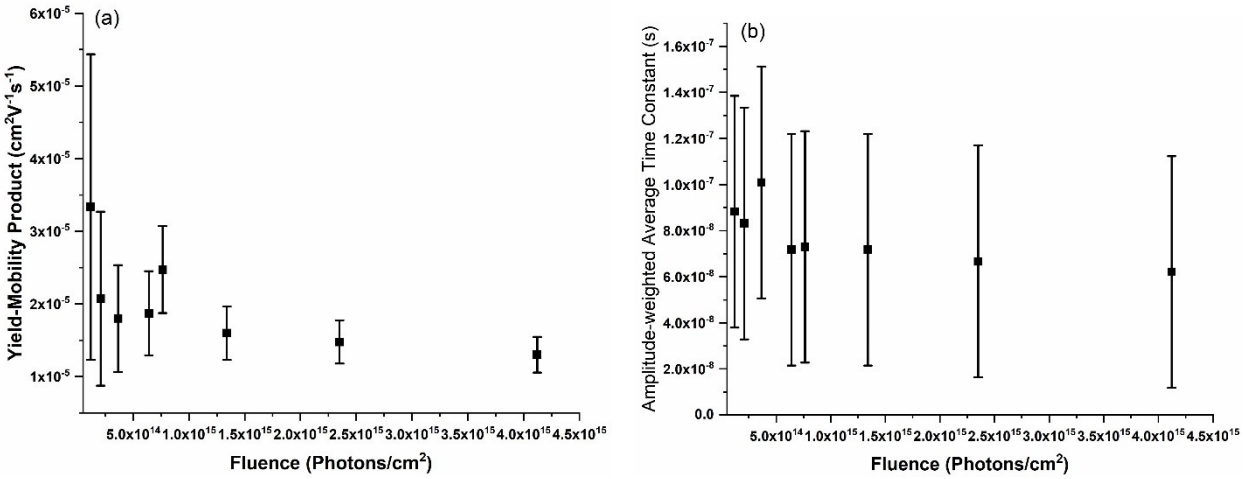

Figure S13. Plots of (a) yield-mobility product, and (b) amplitude-weighted average time constant vs fluence for a ZnPor-COF-PS film.

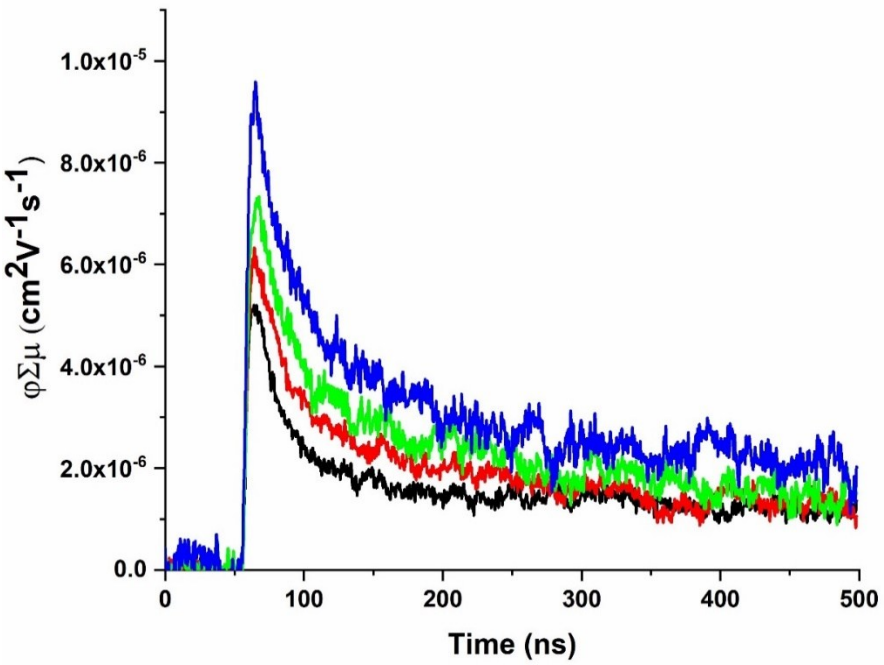

Figure S14. Representative fp-TRMC transients with increasing fluence for a ZnPor-COF-PMMA film at 700 nm photoexcitation.

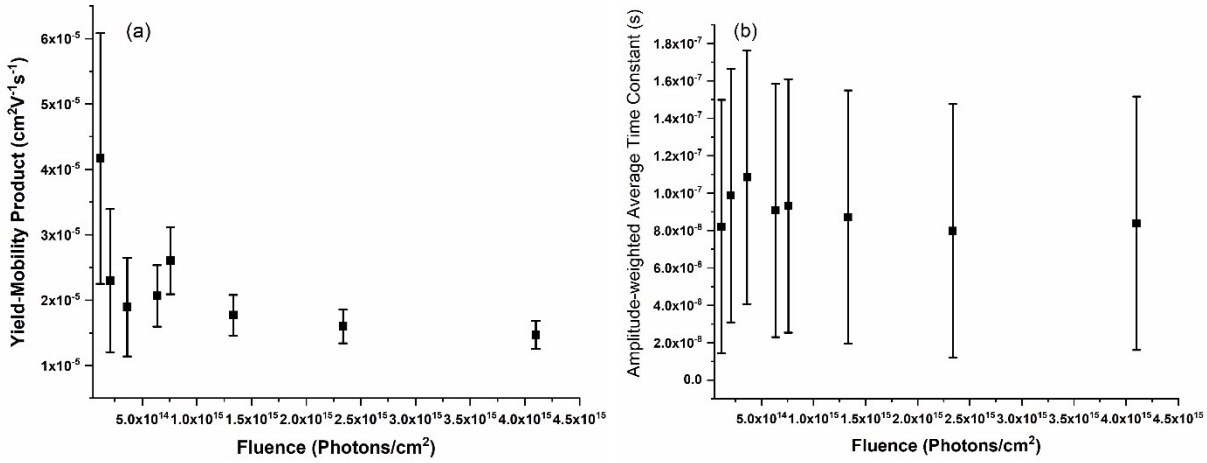

Figure S15. Plots of (a) yield-mobility product, and (b) amplitude-weighted average time constant vs fluence for a ZnPor-COF-PMMA film.

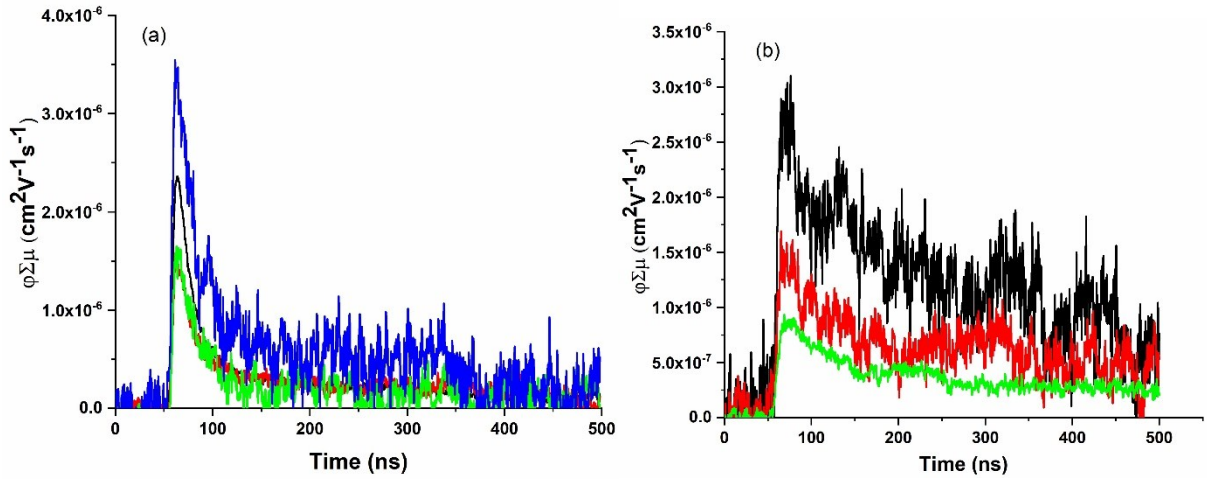

Figure S16. Plot of fp-TRMC transients at different fluences at 430 nm for (a) ZnTPP neat film, and (b) blank quartz slide. Plots show the yield mobility obtained for ZnTPP was on the level of the response of a blank quartz slide, showing no appreciable signal from which mobilities can be estimated. Signal at 550 and 700 nm was progressively weaker and never significantly greater than the quartz background.

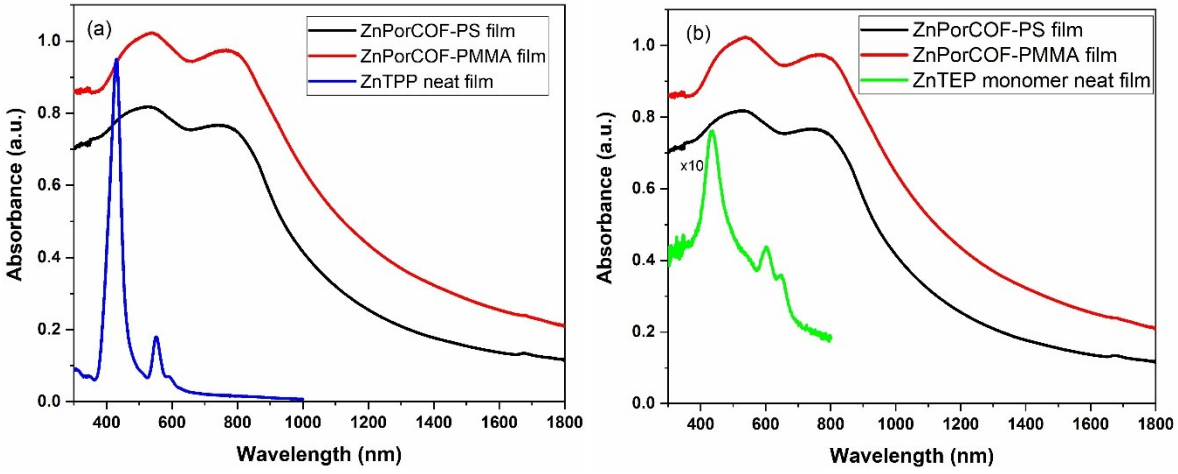

Figure S17. Absorption spectra of ZnPor-COF-polymer blends and (a) ZnTPP film, and (b) ZnTEP film obtained via transmission measurements.

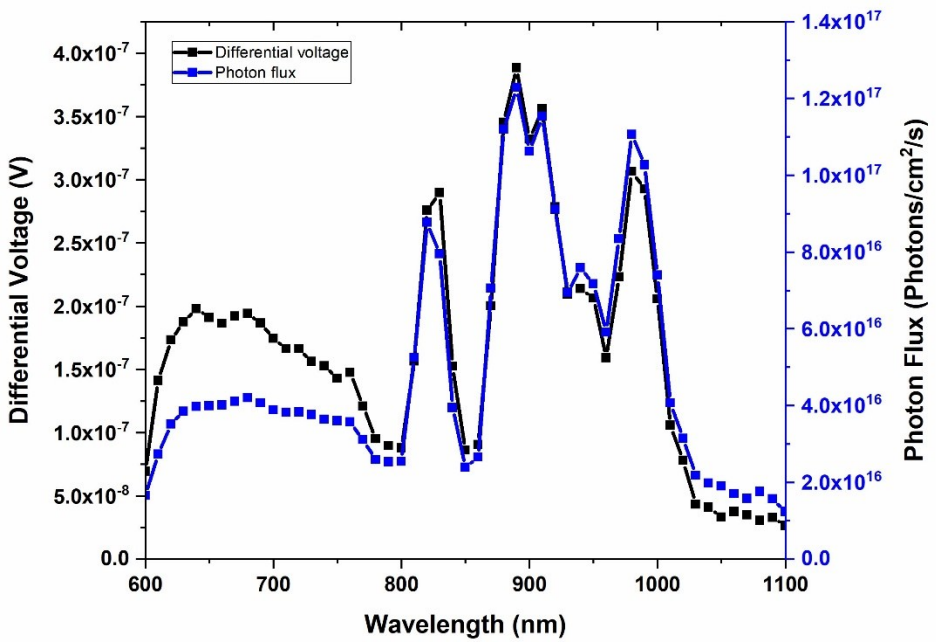

Figure S18. Plots of differential voltage and photon flux vs wavelength for a ZnPor-COF-PMMA film. This plot shows a broadband response photoconductance response that is shown by the differential voltage signal mirroring the output of the xenon arc lamp (shown as photon flux).

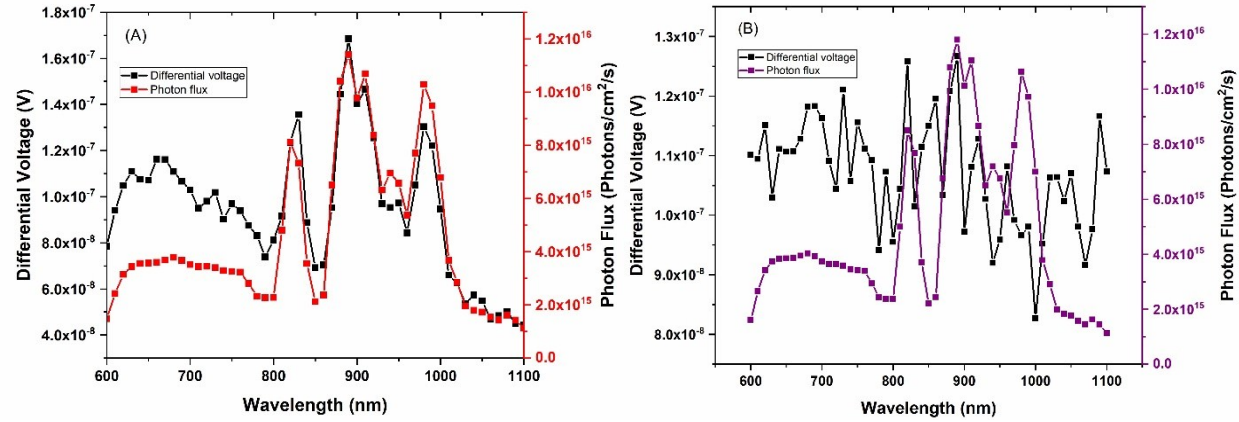

Figure S19. Plots of differential voltage and photon flux vs wavelength for (A) ZnPor-COF-PS film, and (B) blank quartz glass. ZnPor-COF-PS film shows broadband response photoconductance response that is shown by the differential voltage signal mirroring the output of the xenon arc lamp (shown as photon flux). The quartz blank shows no signal as seen in differential voltage curve, which fluctuates $\pm$ 20 nV (noise level) around the baseline offset of ca. 110 nV.

Table S1. Calculated effective masses and their directions for the 2D COFs.

	Hole		Electron	
Pyr-COF	0.13	0.24	0.12	0.26
	Γ-B	Γ-L	Γ-B	Γ-L
Por-COF	0.07	0.09	0.07	
	M-Γ	M-Γ	M-Γ	
ZnPor-COF	0.08	0.10	0.10	
	M-Γ	M-Γ	X- Γ	

Table S2. Nonlocal relaxation energies (L), variance of transfer integrals (σ), and transfer integrals (t) in the 2D COFs.

	L for hole (meV)	**σ (meV)**	**t for hole (meV)**	**L for electron (meV)**	**σ (meV)**	**t for electron (meV)**
pyrene	48	49.8	204	49	50.0	206
Porphyrin	76	62.7	232			
Zn-porphyrin	67	58.9	232			

Table S3. Estimated mobilities for holes (μ_h in $cm^2V^{-1}s^{-1}$) and electrons (μ_e in $cm^2V^{-1}s^{-1}$) in the 2D COFs with and without application of parameter renormalization due to the local electron-vibration couplings.

	Mobility without renormalized parameters		**Mobility with renormalized parameters**	
	μ_h	μ_e	μ_h	μ_e
Pyr-COF	81	81	65	66
Por-COF	90		82	
ZnPor-COF	103		94	

II. Deformation Potential (DP) Calculations

We have calculated the charge-carrier mobilities in the 2D COFs using the deformation potential (DP) theory proposed by Bardeen and Shockley.[8] This theory approximates the electron-phonon couplings through the electron scattering due to longitudinal acoustic phonons. It was applied to 2D systems such as graphene[9], h-BN[10], or MX_2[11] for which it provides an upper bound for the intrinsic mobilities. For a parabolic band, the mobility along direction *i* writes as:

$$\mu_i^{(2D)} = \frac{e\tau}{m_i^*} = \frac{e\hbar^3 C_{11i}^{(2D)}}{k_B T (m_i)^{\frac{1}{2}} (m_x m_y)^{\frac{1}{2}} E_{1i}^2}$$

where the relaxation time (τ) is calculated from deformation potential approach following:

$$\tau = \frac{\hbar^3 C_{11i}^{(2D)}}{k_B T (m_x m_y)^{\frac{1}{2}} E_{1i}^2}$$

where k_B denotes the Boltzmann constant and T, the temperature, which is set at 300K as in similar studies; m_i, C_i, and E_{1i} are the effective mass, elastic modulus, and deformation potential along the i (=x,y) direction. The deformation potential, E_{1i} $\left(= \Delta E_{VB/CB} / \left(\frac{\Delta l}{l_0}\right)\right)$, is calculated from the shifts in the valence or conduction band along the *i* direction of lattice dilation. Similarly, elastic constant C_{11i} is calculated via a parabolic fit of the total energy with respect to volume change for a lattice dilation along *i* as:

$$(E - E_0)/S_0 = \left(\frac{\Delta l}{l_0}\right)^2 \frac{C_{11i}^{(2D)}}{2}.$$

Here, the 2D COF are dilated up to ±1% in steps of 0.5% of optimized lattice constant.

Table S4. Calculated mobilities using DP theory for hole (μ_h in $cm^2V^{-1}s^{-1}$) and electron (μ_e in $cm^2V^{-1}s^{-1}$) in Pyr-COF along the [10]- and [01]-directions, and averaged value of the scattering relaxation time (τ in ps) along with the parameters used in the calculation.

	E_{1x}	E_{1y}	C_{1x}	C_{1y}	$\mu_x^{(2D)}$	$\mu_y^{(2D)}$	τ
Hole	1.47	2.13	30.32	67.29	7,960	4,595	0.6
Electron	1.40	1.60	30.32	67.29	8,860	7,437	0.9

Table S5. Calculated mobilities using DP theory for hole (μ_h in $cm^2V^{-1}s^{-1}$) and electron (μ_e in $cm^2V^{-1}s^{-1}$) in Por-COF along the x- and y-directions, and averaged value of the scattering relaxation time (τ in ps) along with the parameters used in the calculation.

	E_{1x}	E_{1y}	C_{1x}	C_{1y}	$\mu_x^{(2D)}$	$\mu_y^{(2D)}$	τ
Hole	4.43	4.44	63.33	62.95	6,195	6,157	0.3
Electron	1.32	1.31	63.33	62.95	30,072	29,800	2.2

References

1. H. L. Anderson, *Tett. Lett*., 1992, **33**, 1101-1104.
2. W.-N. Yen, S.-S. Lo, M.-C. Kuo, C.-L. Mai, G.-H. Lee, S.-M. Peng and C.-Y. Yeh, *Org. Lett.,* 2006, **8**, 4239-4242.
3. M. J. Plater, S. Aiken, and G. Bourhill, *Tetrahedron*, 2002, **58**, 2415-2422.
4. T. Lange, J.-D. van Loon, R.R. Tykwinski, M. Schreiber, and F. Diederich, *Synthesis*, 1996, **4**, 537-550.
5. P. H. S. Paioti, K. A. Abboud and A. Aponick, *J. Am. Chem. Soc*. 2016, **138**, 2150-2153.
6. Reid, O. G.; Moore, D. T.; Li, Z.; Zhao, D.; Yan, Y.; Zhu, K.; Rumbles, G., *J. Phys. D: Appl. Phys.,* 2017, **50**, 493002.
7. T.J. Savenije, A.J. Ferguson, N. Kopidakis, G. Rumbles, *J. Phys. Chem. C,* 2013, ***117***, 24085-24103.
8. J. Bardeen and W. Shockley, *Phys. Rev.,* 1950, **80**, 72-80.
9. L. Chen, L. Wang, Z. Shuai and D. Beljonne, *J. Phys. Chem. Lett.,* 2013, **4**, 2158-2165.
10. S. Bruzzone, and G. Fiori, *Appl. Phys. Lett.,* 2011, **99**, 222108-222108-3.
11. W. Zhang, Z. Huang, W. Zhang and Y. Li, *Nano Res.,* 2014, **7**, 1731-1737.